

Article

Identifying Key Hydrological Processes in Highly Urbanized Watersheds for Flood Forecasting with a Distributed Hydrological Model

Huanyu Wang and Yangbo Chen *

School of Geography and Planning, Sun Yat-Sen University, Guangzhou 510275, China

* Correspondence: eescyb@mail.sysu.edu.cn; Tel.: +86-20-84114269

Received: 31 July 2019; Accepted: 6 August 2019; Published: 8 August 2019



Abstract: The world has experienced large-scale urbanization in the past century, and this trend is ongoing. Urbanization not only causes land use/cover (LUC) changes but also changes the flood responses of watersheds. Lumped conceptual hydrological models cannot be effectively used for flood forecasting in watersheds that lack long time series of hydrological data to calibrate model parameters. Thus, physically based distributed hydrological models are used instead in these areas, but considerable uncertainty is associated with model parameter derivation. To reduce model parameter uncertainty in physically based distributed hydrological models for flood forecasting in highly urbanized watersheds, a procedure is proposed to control parameter uncertainty. The core concept of this procedure is to identify the key hydrological and flood processes in the highly urbanized watersheds and the sensitive model parameters related to these processes. Then, the sensitive model parameters are adjusted based on local runoff coefficients to reduce the parameter uncertainty. This procedure includes these steps: collecting the latest LUC information or estimating this information using satellite remote sensing images, analyzing LUC spatial patterns and identifying dominant LUC types and their spatial structures, choosing and establishing a distributed hydrological model as the forecasting tool, and determining the initial model parameters and identifying the key hydrological processes and sensitive model parameters based on a parameter sensitivity analysis. A highly urbanized watershed called Shahe Creek in the Pearl River Delta area was selected as a case study. This study finds that the runoff production processes associated with both the ferric luvisol and acric ferralsol soil types and the runoff routing process on urban land are key hydrological processes. Additionally, the soil water content under saturated conditions, the soil water content under field conditions and the roughness of urban land are sensitive parameters.

Keywords: flood forecasting; urbanization; distributed hydrological model; land use/cover; satellite remote sensing

1. Introduction

In the past century, the world has observed large-scale urbanization, and the urban population reached 50% of the total population in 2007 [1]. In recent decades, urbanization in developed countries remains ongoing [2], but it is more rapid in developing countries. For example, China's urban population increased from 19.39% in 1980 to 50% in 2011 [3], and is projected to reach 65% in 2050 [4]. Urbanization in China's south and east coast region is very rapid, and the Pearl River Delta area on the south coast has experienced the most rapid urbanization [5]. This rapid urbanization has resulted in the formation of several international metropolitan areas in this region in just three decades. These metropolises include Guangzhou, Shenzhen, Dongguan, Foshan, Zhongshan and Zhuhai.

The Pearl River Delta area is a waterway-rich area with numerous small watersheds that drain to city centers. This area is located in a monsoon zone with frequent severe storms, thus, flooding is very common and is a threat to urban communities. Notably, floods have caused serious damage and resulted in numerous losses in previous decades. During the urbanization process, the land use/cover (LUC) in these watersheds has changed tremendously. The most common LUC change is the conversion of vegetated areas, such as grassland, farmland and forestry land, into urban land uses, such as roads, factories, residential areas and commercial complexes. Therefore, most of the vegetation has disappeared. Currently, the areal percentage of urban land in a watershed is over 50% in most watersheds [6,7]. Urbanized land comprises impervious surfaces with low infiltration rates and high runoff routing velocities. Studies have shown that urbanization increases surface runoff and peak flow [8–12] and increases flooding and flood damage. In the Pearl River Delta area, this urbanization effect is obvious, and more flood damage and losses have been observed in recent decades [13,14] (e.g., increased economic damages, transportation jams).

Flood forecasting is a cost-effective flood mitigation measure. However, forecasting floods in the highly urbanized watersheds in the Pearl River Delta area is difficult and has not been attempted. Generally, watershed flood forecasts are created using watershed hydrological models. The most widely used watershed hydrological models are lumped models [15,16], which analyze the watershed as a whole. Such models include the Stanford model [17], the Xinjiang model [18] and the ARNO model [19], among others. Lumped models require long series of hydrological observation data to calibrate the model parameters. No discharge observations are available in most of the watersheds in the Pearl River Delta area; however, rain gauges have been installed in most of these watersheds in recent years. Thus, precipitation data are available. Due to rapid urbanization and vegetation change, flood responses have changed considerably, and the associated model parameters have also changed. Therefore, even though discharge data may be available in some watersheds, the calibrated model parameters only represent past scenarios, and a new model parameter is needed to reflect the LUC changes—this is usually not easy. Thus, lumped hydrological models cannot be effectively used for flood forecasting in watersheds in the Pearl River Delta area.

Physically based distributed hydrological models (PBDHMs) are relatively new watershed hydrological models. PBDHMs divide a watershed into grid cells [20–22], and hydrological processes are calculated at the cell scale. Thus, they have the potential to better simulate and predict watershed hydrological processes [23]. Dozens of PBDHMs have been proposed, such as the System Hydrologique Européen model (SHE) proposed by Abbott et al. [21,22], the flood forecasting system model (WATERFLOOD) proposed by Kouwen [24], the terrain-based model (THALES) proposed by Grayson et al. [25], the variable infiltration capacity model (VIC) proposed by Liang et al. [26], the distributed hydrology-vegetation model (DHSVM) proposed by Wigmosta et al. [27], the raster-based hydrologic model (CASC2D) proposed by Julien et al. [28], the water and energy transfer between soil, plants and atmosphere model (WetSpa) proposed by Wang et al. [29], the geomorphology-based hydrologic model (GBHM) proposed by Yang et al. [30], the water and energy transfer process (WEP) model proposed by Jia et al. [31], the gridded, physics-based hydrologic model (Vflo) proposed by Vieux and Vieux [32], the watershed environmental hydrology (WEHY) model proposed by Kavvas et al. [33,34] and the Liuxihe model (LXH) proposed by Chen et al. [16], among others.

PBDHMs derive model parameters physically from watershed terrain properties, including elevation, soil type and LUC. Therefore, model parameters do not need to be calibrated using observed hydrological data, thus requiring less calibration efforts. Based on these advantages, PBDHMs can be used to model watersheds in the Pearl River Delta area. The largest challenge associated with physically deriving the model parameters of a PBDHM is the inherent uncertainty. Since PBDHMs derive model parameters physically, model parameter uncertainty exists, and various measures are needed to control this parameter uncertainty [35–38]. Some general methodologies and frameworks for assessing uncertainties of hydrological modeling have been proposed already. For example, Apel et al. [39] developed a stochastic flood risk model which can consider risk and uncertainty associated with the very

components of the hydrological process and Moradkhani et al. [40] proposed a sequential hydrologic data assimilation approach using particle filters for estimating model parameters, state variables and assessing related uncertainty. Liu et al. [41] presented an integrated hierarchical framework for reducing uncertainty in hydrologic predictions. Hall et al. [42] proposed a dynamic-probabilistic method for cumulated flood risk assessment of a complete river reach, and Beven [43] discussed the uncertainty sources and suggested the use of a condition tree to assess it. While these studies are more general on methodologies, several methods have been proposed for controlling model parameter uncertainty by optimizing them, such as the scalar method [44,45] in the Vflo model, the Shuffle Complex Evolution (SCE) algorithm in MIKE SHE (European hydrological system) [35], the multi-objective genetic algorithm in the WetSpa model [46], the Shuffle Complex Evolution–University of California (SCE-UA) algorithm [47] and the Particle Swarm Optimization (PSO) algorithm [38] in the Liuxihe model. Previous studies have shown that parameter optimization is recommended if reliable observation data are available, even if the data are limited [38]. However, this process is difficult in the Pearl River Delta area because no river discharge observations are available. Therefore, although a PBDHM could be used for flood forecasting in the highly urbanized watersheds of the Pearl River Delta area, there is currently no way to effectively control parameter uncertainty.

Based on the above analysis, further studies are needed for exploring effective ways to control parameter uncertainty of a PBDHM for flood forecasting in the highly urbanized watersheds of the Pearl River Delta area. In this study, the explored science question is which hydrological processes are key in modeling highly urbanized watershed floods in the Pearl River Delta area. If the key flood hydrological processes are known, then efforts could be put on the uncertainty controlling of the parameters related to these key flood hydrological processes. We proposed a procedure to identify the key flood hydrological processes in the highly urbanized watersheds by parameter sensitivity analysis, and determined the most sensitive model parameters related to these key processes. Next, we proposed some measures for controlling the parameter uncertainty. A highly urbanized watershed called Shahe Creek in Guangzhou city, the capital city of the Pearl River Delta area, was selected as a case study. The results indicate that the proposed method is useful in controlling the parameter uncertainty of the Liuxihe model in flood forecasting for highly urbanized watersheds in the Pearl River Delta area.

2. Methodology

2.1. General Methodology

In this paper, a highly urbanized watershed is a watershed in which urbanized land is the dominant type of land cover (i.e., the areal percentage of urbanized land cover in the watershed drainage area is larger than the percentages of all other land cover types and generally higher than 30%). In the Pearl River Delta area, most of the watersheds that drain to the city are highly urbanized watersheds with areal percentages of urban land greater than 30% [48–50].

In this study, we propose that only a few hydrological processes are important in these highly urbanized watersheds, and the key ones are related to the dominant LUCs. Additionally, the key hydrological processes are different from the dominant ones in this study. Dominant hydrological processes are those that control the flood formation in the entire basin, such as rainfall-runoff production and runoff routing. To accurately simulate the floods in each watershed, these hydrological processes should be calculated properly. Key hydrological processes in this paper are also dominant hydrological processes, but they are difficult to accurately calculate, particularly when determining the model parameters related to them. If a dominant hydrological process could be accurately calculated using current methods or data, then it is not a key hydrological process. Numerous model parameters are needed to simulate flood at the watershed scale using a distributed hydrological model, and the uncertainty associated with these model parameters can be high if the parameters are not optimized. Therefore, by focusing on only a few key hydrological processes in these highly urbanized watersheds,

more attention can be given to accurately determining the model parameters related to these key hydrological processes in a manner that reduces the associated uncertainty.

The core concept of the approach proposed in this article is to identify the key hydrological processes and the sensitive model parameters related to these key hydrological processes. One key hydrological process should be related to urbanized land, as it is the dominant LUC. In the Pearl River Delta area, LUC is generally categorized into six types: urbanized land, farmland, forestry land, grassland, bare land and water bodies. In most cases, bare land and water bodies are not dominant LUCs; thus, no more than four dominant LUCs exist. After identifying the key hydrological processes, the key model parameters (i.e., the sensitive model parameters), should be identified and carefully determined to reduce the associated uncertainty. In this paper, a parameter sensitivity analysis is used to identify the sensitive parameters. The following procedure was used:

1. Collect LUC information in watershed by satellite or ground-based method. It is highly recommended that the latest LUC be estimated using the latest satellite remote sensing imagery, and numerous automated algorithms have been developed for LUC data extraction. The support vector machine (SVM) algorithm is used in this study; details of the algorithm are provided in Section 2.3.
2. Analyze the LUC spatial pattern in the watershed and calculate the areal percentage of each LUC type.
3. Identify the dominant LUC types and their spatial structures, and propose the key hydrological processes based on the dominant LUC types.
4. Choose one distributed hydrological model as the forecasting tool. Any physically based distributed hydrological model can be used. In this study, the Liuxihe model is employed and will be discussed in Section 2.2. The initial model parameters are then derived physically from the terrain properties.
5. A parameter sensitivity analysis is performed for each key hydrological process. Then, the key model parameters of each key hydrological process are identified. The parameter sensitivity analysis used in this study is the one-factor-at-a-time (OAT) method, which will be introduced in detail in Section 2.4.
6. After identifying the key model parameters, methods to control model parameter uncertainty may be used to optimize the initial model parameters. Only key model parameter values will be adjusted, and other parameters will maintain their initial values.

2.2. Liuxihe Model and Hydrological Processes

The distributed hydrological model recommended in this paper is the Liuxihe model. The Liuxihe model is a physically based, distributed watershed hydrological model that was initially proposed for watershed flood forecasting [16,38,51]. In the Liuxihe model, the evaporation process is not a key flood generation process, and the parameters related to this process are less sensitive parameters, including the potential evaporation capacity and evaporation coefficient [16]. In this study, this conclusion is adopted, and the sensitivities of these parameters are not studied.

Runoff production is regarded as a key hydrological process in modeling flood processes, and the parameters related to this process are soil-based parameters, such as soil hydraulic conductivity, soil water content under saturated conditions, soil water content under field conditions, soil water content under wilting conditions, soil layer thickness and soil property coefficients. The soil water content under wilting conditions and soil property coefficients are less sensitive parameters in flood process modeling [16].

Runoff production is mainly related to soil type, and there are generally multiple soil types in a watershed. Therefore, the runoff production process is further divided into soil type-related runoff production processes in this study. The runoff production processes related to the dominant soil types

may be dominant hydrological processes, as the soil type parameters should not be determined easily. Thus, the dominant runoff production processes may be key hydrological processes.

Runoff routing is regarded as another key hydrological process in flood process modeling. Parameters related to this process are vegetation-based parameters, including the LUC roughness and river channel roughness. Since river channels do not change much and can be evaluated relatively easily, river channel runoff routing is not considered a key hydrological process, although it is a dominant hydrological process in runoff routing. Thus, in this article, only hill slope runoff routing is regarded as a key hydrological process. As there are generally several vegetation types on the slopes within a watershed, hill slope runoff routing processes related to the dominant LUCs are key hydrological processes.

2.3. SVM Algorithm for LUC Estimation

The traditional method of mapping LUC is based on field investigation, but mapping at the watershed scale is time consuming, costly and not feasible for flood forecasting. However, estimating LUC with satellite remote sensing imagery provides a cost-effective method of mapping LUC. LUC estimation with satellite remote sensing images can be performed with automatic classification algorithms, which can be categorized as supervised classification algorithms, unsupervised classification algorithms and semi-supervised classification algorithms. Supervised classification algorithms can be further divided into statistical algorithms [52], decision tree algorithms [53], artificial neural networks [54] and support vector machine (SVM) algorithms [55–57]. Unsupervised classification algorithms can be further divided into K-means algorithms [58], fuzzy c-means algorithms [59] and Affinity Propagation (AP) clustering algorithms [60]. Semi-supervised classification methods can improve an algorithm's performance by utilizing non-tagged samples [61–64]. SVM is a machine learning method proposed by Vapnik [65]. In this method, training data are mapped to a higher dimension to find an optimal hyperplane that separates the tuples tagged in the same class from others. SVMs are highly robust, not affected by the addition or removal of samples from the support vector, highly accurate for modeling complex nonlinear decision boundaries and able to avoid overfitting. Additionally, SVMs have been widely used for LUC classification [57]. Past studies have shown that SVMs provide better classification accuracy [66,67]. In this study, an SVM algorithm is employed to estimate the LUC in the studied watershed.

2.4. OAT Method for Parameter Sensitivity Analysis

In this study, the one-factor-at-a-time (OAT) approach is used in the parameter sensitivity analysis. Based on the OAT method, parameter sensitivity analysis is performed for one parameter at a time. If the analysis is performed to assess the relative importance of each input factor, then this method is suitable [68]. If there are m parameters, where $i = 1, 2, \dots, m$; and for every parameter, it takes n values, where $j = 1, 2, \dots, n$; then the sensitivity factor of the i th parameter is defined as follows:

$$SF_i = \frac{Sim_{j+1,i} - Sim_{j,i}}{p_{j+1,i} - p_{j,i}} \quad (1)$$

where SF_i is the sensitivity factor of the i th parameter with no units, $p_{j,i}$ is the perturbation value of the i th parameter with the same units as the parameter, and $Sim_{j,i}$ is the simulation index of the i th parameter with parameter value $p_{j,i}$, and the units are dependent on the simulation index. Generally, p includes multiple values within its feasible range. The parameters with high SF values are defined as highly sensitive parameters (i.e., slight changes in these parameters will produce significant changes in model simulation results). Thus, these parameter values must be carefully determined.

In this study, two simulation indices are recommended for the sensitivity analysis. One is the peak discharge (i.e., the maximum river channel flow at the watershed outlet). The other is the runoff coefficient of a flood event, which can be defined as follows:

$$E_k = 3.6 \sum_{t=1}^T Sim_{t,k} / A \sum_{t=1}^T P_{t,k} \quad (2)$$

where E_k is the runoff coefficient of the k th flood event simulated based on the parameters in the sensitivity analysis (no units), $P_{t,k}$ is the watershed-averaged precipitation at stage t of flood event k (the units of k and t are mm and hours, respectively) and there are T stages in flood event k . $Sim_{t,k}$ is the simulated river channel flow at the watershed outlet during stage t of flood event k (units of m^3/s). A is the drainage area of the entire watershed (units of km^2), and 3.6 is a unit conversion coefficient.

3. Study Watershed and Data

3.1. Study Watershed

Shahe Creek in Guangzhou city was selected as the study watershed. Shahe Creek originates in the northern part of Guangzhou city and drains into the city center where it merges with the Pearl River. Shahe Creek has a drainage area of $32.9 km^2$ and a length of 15 km. It is the largest watershed that drains to the city center directly and is the most direct flood threat to Guangzhou city. Figure 1 shows a map of Shahe Creek.

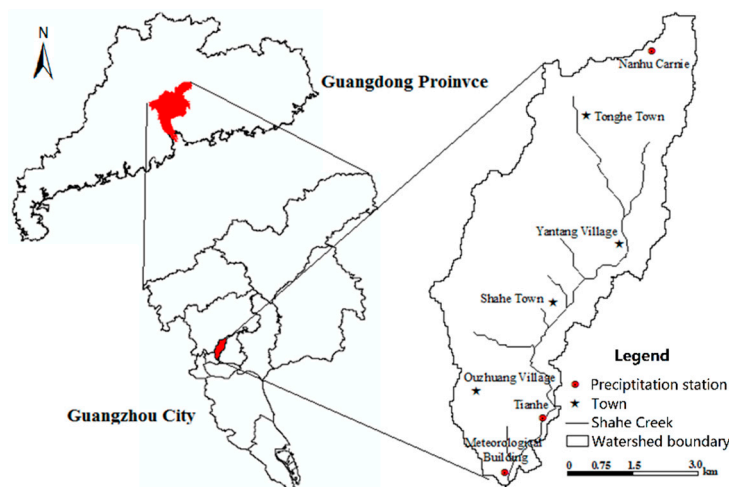


Figure 1. Map of the Shahe Creek watershed.

Shahe Creek is located in a tropical area with an average annual precipitation of 1725 mm. Flooding is mainly induced by storms in the monsoon season, and floods are very frequent. In past decades, Shahe Creek has experienced rapid urbanization, which has created a high percentage of urbanized land. It is a typical watershed in the Pearl River Delta area that experiences considerable flooding (e.g., the flood events in June 2017, May 2016 and June 2015).

3.2. Hydrological Data

Three rain gauges have been installed in the watershed in recent years, and their locations are shown in Figure 1. In this study, precipitation data were collected at hourly intervals during three storm events that occurred in 2015 and 2016, and the Thiessen polygons method was employed for interpolation. Table 1 shows the basic storm information; no river discharge data are available for these events.

Table 1. Storm event information.

Storm Event No.	Start Time (yyyyymmddhh)	End Time (yyyyymmddhh)	Duration (h)	Total Rainfall (mm)	Storm Scale
20150111	2015011118	2015011317	47	42.6	Light
20150516	2015051607	2015051703	20	47.23	Medium
20160128	2016012813	2016012914	25	83.96	Heavy

3.3. Estimating LUC with Satellite Remote Sensing Imagery

In this study, the Landsat 8 satellite [69,70] remote sensing imagery taken on 3 January, 2015 was downloaded from the U.S. Geological Survey (USGS) website to estimate the LUC in the Shahe Creek watershed. The high-quality imagery covers all of Shahe Creek. The downloaded imagery was preprocessed, including noise filtering, radiation correction, atmospheric correction, georeferencing and enhancement. Six LUC types, including urban land (impervious surfaces), water bodies, forestry land, farmland, grassland and bare land were used in the classification. The LUC of Shahe Creek in 2015 was first estimated by employing an SVM algorithm and then post-processed via manual interpretation to increase the classification accuracy. Figure 2a shows the original imagery of Shahe Creek in 2015, while Figure 2b shows the estimated LUC after post-processing, which is used in the following analyses.

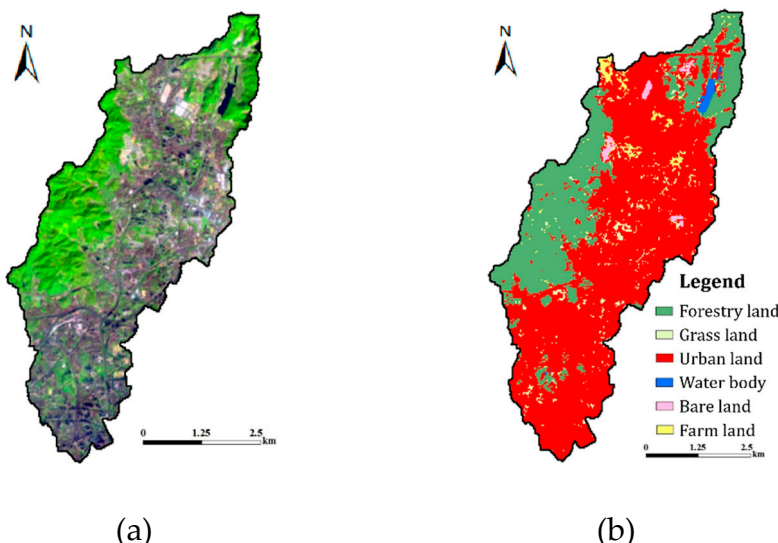


Figure 2. Landsat imagery and estimated land use/cover (LUC) of the Shahe Creek watershed in 2015. (a) Preprocessed Landsat 8 imagery (taken on 3 January 2015); (b) estimated LUC result (estimated with a support vector machine (SVM) and post-processed).

3.4. Dominant LUC Types

Based on the results in Figure 2, urban land dominates the LUC at 59.73%, (i.e., more than half of the watershed has been converted to impervious surfaces). Thus, the watershed is highly urbanized. The urban land in Shahe Creek is mainly located in the middle and downstream reaches, which are completely urbanized. The second largest LUC is forestry land at 28.67%. The majority of forestry land is located in the upper reach, which is a mountainous area. Farmland comprises 5.48% of the watershed and is mainly used to grow vegetables for the inhabitants of Guangzhou city, as much of this land is close to the city center. Additionally, grassland comprises 4.76% of the watershed, while bare land and water bodies comprise 0.78% and 0.58%, respectively.

4. Liuxihe Model and Initial Parameters

4.1. Watershed Terrain Property Data

Watershed terrain property data are required to establish a PBDHM and derive its parameters, which include Digital Elevation Models (DEMs), soil maps, LUC maps, river channel shapes, cross sections and sizes. In this study, a DEM was derived from a recent contour map at a spatial resolution of 30 m, as shown in Figure 3a. The Shahe Creek watershed has an average elevation of 54.24 m, with a maximum elevation of 370 m and minimum elevation of 3.90 m.

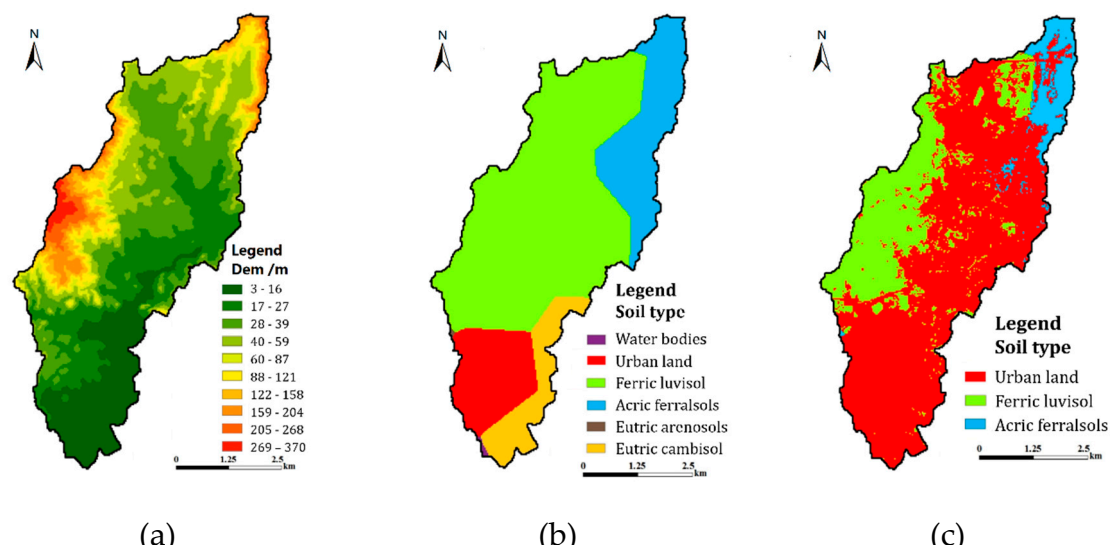


Figure 3. Terrain property data in the Shahe Creek watershed. (a) DEM; (b) soil map (downloaded from the FAO website); (c) soil map (updated using the LUC estimated based on satellite remote sensing imagery).

The soil types in Shahe Creek were extracted from the Food and Agriculture Organization (FAO) world soil map dataset, as shown in Figure 3b. There are six soil types in the watershed, including water bodies, urban land, ferric luvisols, acric ferralsols, eutric arenosols and eutric cambisols, with areal percentages of 0.158%, 12.592%, 60.918%, 17.443%, 0.060% and 8.829%, respectively. Note that the urban land soil type is a virtual soil type proposed by the author, for which the LUC is urban land, but the actual soil type could be any one. The FAO data are not the most recent data, and some urban land has changed since the data were prepared. Therefore, in this study, the soil type map is updated using the LUC estimation in this study (Figure 2), as shown in Figure 3c. After this update, only three soil types were observed, including urban land, ferric luvisols and acric ferralsols, with areal percentages of 59.73%, 31.21% and 9.06%, respectively.

4.2. Liuxihe Model Set-Up

The DEM produced in this study with a spatial resolution of 30 m was used to divide the studied watershed into 34,919 grid cells, which were further divided into 700 river cells and 34,219 hill slope cells. A three-order river network was derived using the D8 method [71,72] and Strahler river ordering method [73] based on the DEM. The river network was further divided into 16 virtual sections based on 8 virtual nodes. In the Liuxihe model, the virtual river cross section shape was assumed trapezoidal, and the river size was estimated based on satellite remote sensing images. The structure of the Liuxihe model for Shahe Creek is shown in Figure 4, and the estimated cross section size is given in Table 2.

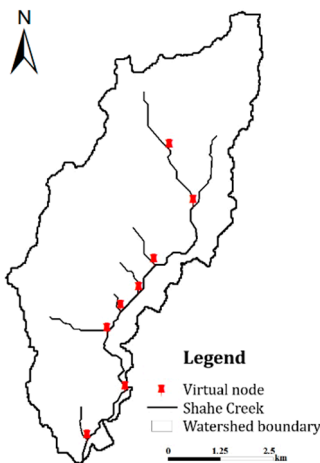


Figure 4. Structure of the Liuxihe model of Shahe Creek.

Table 2. Estimated cross section size and parameters.

ID	Bottom Width (m)	Side Slope (degree)	Bottom Slope (no unit)	Roughness (s/m^(1/3))
11	5.0	30	0.00687	0.025
12	2.0	30	0.00024	0.025
13	2.0	30	0.00262	0.025
14	2.2	30	0.01112	0.025
15	2.5	30	0.00496	0.025
16	3.0	30	0.01213	0.025
17	3.0	30	0.00883	0.025
18	3.0	30	0.00333	0.025
21	9.0	30	0.00821	0.025
22	9.0	30	0.0010	0.025
23	9.35	30	0.0010	0.025
24	11.9	30	0.00187	0.025
25	15.9	30	0.001	0.025
26	16.7	30	0.00489	0.025
27	24.7	30	0.00205	0.025
28	16.0	30	0.00071	0.025

4.3. Determination of the Initial Model Parameters

In the Liuxihe model, flow direction and slope are two topography-based model parameters, derived using the D8 method [71,72] based on the DEM. The results are shown in Figure 5.

The only climate-based parameter is the evaporation capacity, which is estimated as 5 mm/day in each grid cell according to daily evaporation observations in this region. The vegetation-based parameters include the evaporation coefficient and roughness. According to previous studies of Liuxihe model parameterization and references [74–78], ranges of vegetation-based parameters are proposed, and the recommended values of the parameters are listed in Table 3. The parameters' values are in physically reasonable ranges, so they could be used in this study.

There are six soil-based parameters, including the soil water content under saturated conditions, the soil water content under field conditions, the soil water content under wilting conditions, the soil layer thickness, the soil hydraulic conductivity at saturation and the soil characteristic coefficient. Based on past modeling studies [7,79–82], the soil water content under wilting conditions is 30% of the soil water content under saturated conditions, and the soil characteristic coefficient is 2.5. Based on local observations, the estimated soil layer thickness is listed in Table 4.

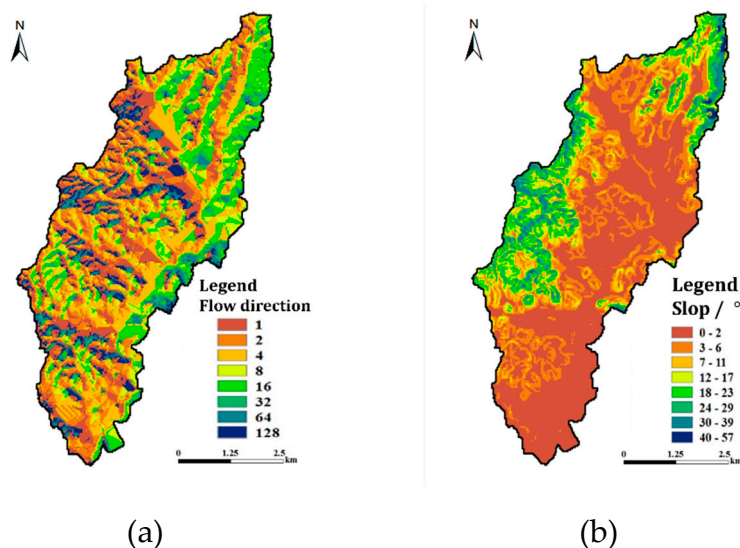


Figure 5. Topography-based model parameters of the Liuxihe model of Shahe Creek. (a) Flow direction; (b) slopes of hill slope cells (degree).

Table 3. Vegetation-based parameter range and recommended values.

Vegetation	Range of Evaporation Coefficient (no unit)	Recommended Evaporation Coefficient (no unit)	Range of Roughness ($s/m^{(1/3)}$)	Recommended Roughness ($s/m^{(1/3)}$)
Forestry land	0.5–0.8	0.7	0.1–0.8	0.55
Grassland	0.5–0.7	0.6	0.01–0.4	0.18
Urban land	0.7–1.3	1.0	0.001–0.2	0.01
Bare land	0.2–0.6	0.4	0.005–0.3	0.12
Farmland	0.4–0.7	0.55	0.02–0.5	0.36

Table 4. Soil-based parameters.

Soil Type	Soil Water Content under Saturated Conditions (%)	Soil Water Content under Field Conditions (%)	Soil Hydraulic Conductivity under Saturated Conditions ($mm \cdot h^{-1}$)	Soil Layer Thickness (mm)
Urban land	0.070	0.010	0.010	1
Ferric luvisols	0.461	0.265	20.828	1500
Acric ferralsols	0.458	0.353	2.794	850

In the Liuxihe model, the Soil Water Characteristics Hydraulic Properties Calculator proposed by Arya et al. [83] was employed to derive the soil water content under saturation conditions, the soil water content under field conditions and the hydraulic conductivity under saturation conditions based on the soil texture, organic matter content, gravel content, salinity and compaction. The estimated parameters are listed in Table 4.

In grid cells with urban land, the surface is impervious (i.e., no infiltration can occur via this surface, and all precipitation is converted to surface runoff). To reflect this hydrological response of urban land, the soil-based parameters of urban land must correspond to this characteristic. In this paper, the soil water content under saturated conditions is assigned a small value, as listed in Table 4. This small value suggests that most of the precipitation that falls onto urban land will be converted into surface runoff, but a small fraction of precipitation will infiltrate or be stored on the surface of urban land cells.

Finally, the roughness of the river channel is estimated based on reference values [7,83], as listed in Table 2.

5. Identify Key Hydrological Processes

5.1. General Analysis of Key Hydrological Processes

In the discussion of Section 2.2, it is concluded that runoff production processes related to the dominant soil types and hill slope routing processes related to the dominant LUCs are potential key hydrological processes. For runoff production, it is divided into runoff production process on both urban land and vegetated lands. As discussed in Section 4.3, the runoff production on urban land is such that all net precipitation fallen on urban land will be converted into surface runoff, and routing as hill slope runoff routing to the river channels. So, the runoff production process on urban land is not a key process in flood forecasting, though it is one of the dominant hydrological processes. Sensitivity analysis of parameters related to this process will not be done as these parameters could be determined reasonably and the uncertainty is low. For runoff production processes on the vegetated lands, those which occurred on the dominant soil types are potential key hydrological processes. Except for urban land soil type, there are only two other soil types, including ferric luvisol and acric ferralsols, so parameter sensitivity related to these soil types will be done to determine the key runoff production hydrological processes.

Urban land is the dominant LUC, forestry land accounts for a big percentage, farmland and grassland account for a small portion, and bare land and water body only account for a very small portion. Therefore, hill slope runoff routing related to urban land and forestry land is the potential key hydrological process, but in this paper, the hill slope runoff routing related to urban land, forestry land, farmland, grassland and bare land will also be studied with parameter sensitivity analysis to determine the key runoff routing hydrological processes.

5.2. Identifying Key Runoff Production Processes

As discussed above, to identify the key runoff production processes, sensitivity analyses are performed for soil-based parameters to identify the sensitive parameters. The analyzed parameters include the soil water content under saturation conditions, the soil water content under field conditions, the soil layer thickness and the soil hydraulic conductivity under saturation conditions. Parameters are analyzed individually and by soil type. Only the parameters of the following two soil types are studied in detail: ferric luvisols and acric ferralsols.

5.2.1. Parameter Sensitivity of Ferric Luvisols

Sensitivity analyses were performed for four parameters individually. The parameters related to ferric luvisol soils were analyzed first. All parameters were assigned 10 values, which is a percentage of the recommended value as listed in Table 4. For different parameters, these percentages are different, and are shown in Figure 6. In this practice, all the perturbated model parameters should still have a physical meaning. The flood discharge values of the three observed flood events were then simulated using observed precipitation and the model parameters. Simulated hydrographs with different ferric luvisol soil-based parameters are shown in Figure 6. Due to manuscript length limitations, only the simulation results for flood event 20160128 are listed. Additionally, only the results of flood event 20160128 are analyzed further.

Figure 6 shows that only the changes in the soil water content under saturation conditions and the soil water content under field conditions have obvious effects on the simulated hydrological processes. Thus, among the soil-based parameters of ferric luvisols, these are the sensitive parameters, and their values must be selected carefully. Based on the above results, the sensitivity factors of the soil water contents under saturation conditions and field conditions are calculated and listed in Table 5. These sensitivity factors are only calculated for peak flow and the runoff coefficient.

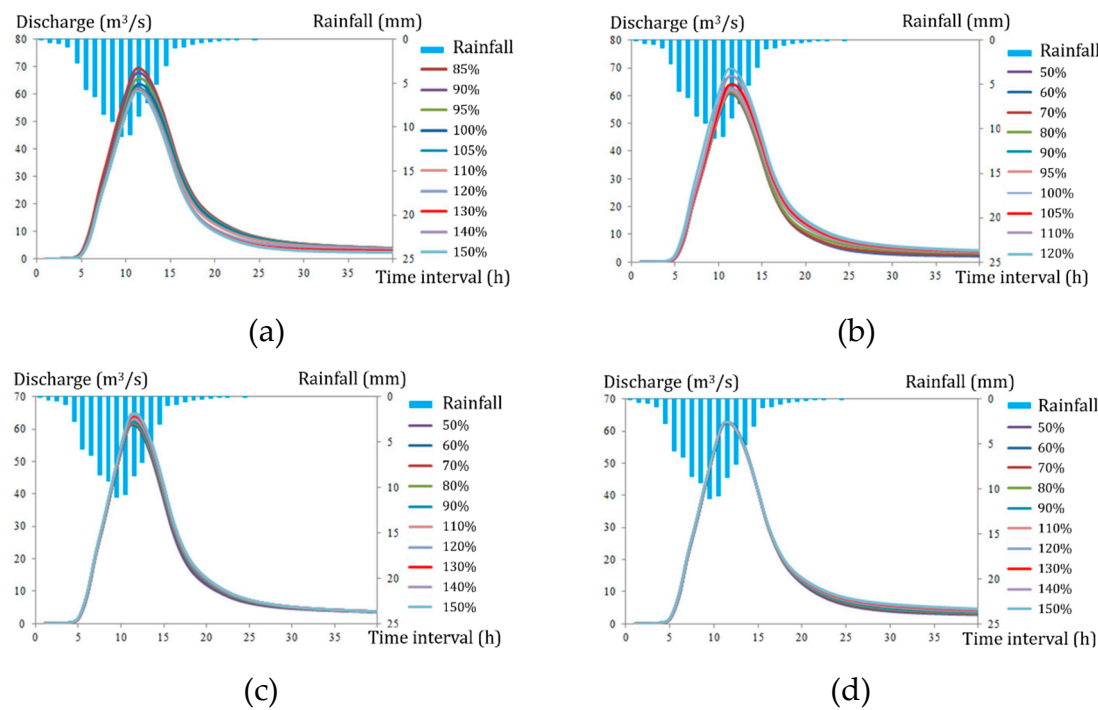


Figure 6. Simulated hydrographs of the soil-based parameter sensitivity analysis of ferric luvisols (flood event 20160128). (a) Soil water content under saturation conditions; (b) soil water content under field conditions; (c) soil hydraulic conductivity under saturation conditions; (d) soil layer thickness.

Table 5. Sensitivity analysis results of ferric luvisols soil-based parameter.

ID	Value (%)	Peak Flow ($\text{m}^3 \cdot \text{s}^{-1}$)	Sensitivity Factor of Peak Flow ($\text{m}^3 \cdot \text{s}^{-1} \cdot \%^{-1}$)	Runoff Coefficient (no unit)	Sensitivity Factor of the Runoff Coefficient (%)
Soil water content under saturation conditions					
1	0.39185	68.82		0.947	
2	0.4149	67.10	-74.55	0.918	-1.25
3	0.43795	65.32	-76.97	0.891	-1.16
4	0.461	63.17	-93.37	0.866	-1.08
5	0.4841	61.68	-64.79	0.844	-0.99
6	0.5071	61.23	-19.43	0.823	-0.90
7	0.5532	60.89	-7.35	0.787	-0.78
8	0.5993	60.69	-4.26	0.763	-0.52
9	0.6454	60.56	-2.83	0.749	-0.29
10	0.6915	60.48	-1.84	0.743	-0.13
Average			-38.376		-0.789
Soil water content under field conditions					
1	0.128	60.34		0.737	
2	0.1536	60.44	3.99	0.745	0.30
3	0.1792	60.60	6.08	0.761	0.63
4	0.2048	60.85	9.79	0.789	1.08
5	0.2304	61.26	15.93	0.825	1.42
6	0.2432	61.40	10.94	0.832	0.55
7	0.256	62.11	55.63	0.852	1.53
8	0.2688	63.68	122.94	0.873	1.63
9	0.2816	66.44	215.08	0.912	3.09
10	0.3072	69.19	107.45	0.962	1.98
Average			60.87		1.35

Table 5 shows that for the entire range of soil water contents under saturation conditions, the decreases in the simulated peak flow and runoff coefficient are $8.34 \text{ m}^3/\text{s}$ and 0.204, respectively, which are 12.12% and 21.54% decreases compared to their baseline values (ID = 1). The average sensitivity factor of peak flow is -38.376 , and the average sensitivity factor of the runoff coefficient is -0.789 . Thus, as the soil water content under saturation conditions increases, the peak flow and runoff coefficient decrease, and the soil water content under saturation conditions is more sensitive to the runoff coefficient.

For the entire range of values of the soil water content under field conditions, the increases in the simulated peak flow and runoff coefficient are $8.85 \text{ m}^3/\text{s}$ and 0.225, respectively, which are 14.67% and 30.53% increases compared to their baseline values (ID = 1). The average sensitivity factor of simulated peak flow is 60.87 , and the sensitivity factor of the runoff coefficient is 1.35 . Thus, as the soil water content under field conditions increases, the peak flow and runoff coefficient increase, and the soil water content under field conditions is more sensitive to the runoff coefficient.

The simulation results of the other two flood events yielded similar conclusions (i.e., soil water content under saturation conditions and soil water content under field conditions are sensitive parameters among the soil-based parameters of ferric luvisols). Due to manuscript length limitations, these results are not presented.

Based on the above results and discussion, the runoff production process associated with ferric luvisol soils is a key hydrological process, and the soil water content under saturation conditions and soil water content under field conditions are sensitive parameters.

5.2.2. Parameter Sensitivity of Acric Ferralsols

Using the same method as described above, the three flood events were simulated with different acric ferralsol-related parameters. Since the results are similar to those of ferric luvisol-related parameters, only the simulated soil water content under saturation conditions and soil water content under field conditions of flood event 20160128 are shown in Figure 7a,b and the other results are not presented.

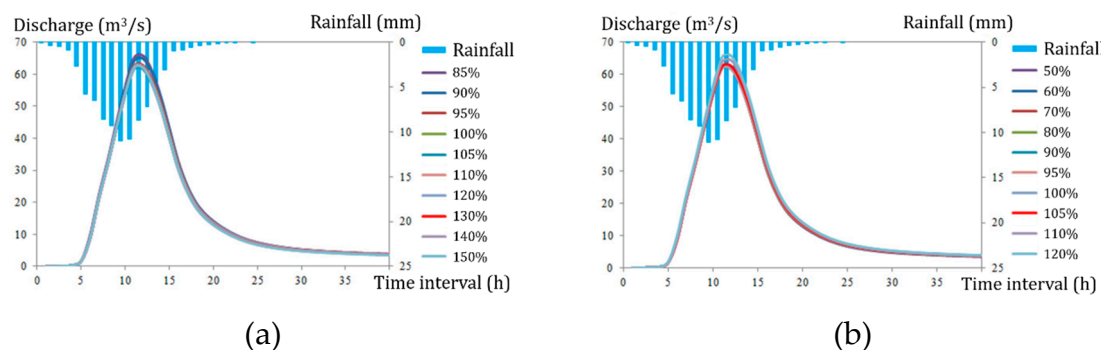


Figure 7. Simulated hydrographs of the soil-based parameter sensitivity analysis of acric ferralsols (flood event 20160128). (a) Soil water content under saturation conditions; (b) soil water content under field conditions.

Figure 7 illustrates that the soil water content under saturation conditions and soil water content under field conditions are sensitive parameters. The sensitivity factors of the soil water content under saturation conditions and soil water content under field conditions were calculated, and they are listed in Table 6.

Table 6. Sensitivity analysis results of acric ferralsols soil-based parameter.

ID	Value (%)	Peak Flow ($\text{m}^3 \cdot \text{s}^{-1}$)	Sensitivity Factor of Peak Flow ($\text{m}^3 \cdot \text{s}^{-1} \cdot \%^{-1}$)	Runoff Coefficient (no unit)	Sensitivity Factor of the Runoff Coefficient ($\% \cdot \%^{-1}$)
Soil water content under saturation conditions					
1	0.3893	65.85		0.892	
2	0.4122	64.92	-40.67	0.883	-0.41
3	0.4351	62.85	-90.20	0.860	-1.00
4	0.458	62.11	-32.54	0.852	-0.34
5	0.4809	61.67	-19.17	0.850	-0.08
6	0.5038	62.40	32.02	0.848	-0.09
7	0.5496	62.19	-4.57	0.846	-0.04
8	0.5954	62.14	-1.10	0.840	-0.12
9	0.6412	62.12	-0.60	0.837	-0.07
10	0.687	62.10	-0.38	0.835	-0.04
Average			-17.469		-0.245
Soil water content under field conditions					
1	0.1765	62.08		0.835	
2	0.2118	62.10	0.60	0.837	0.07
3	0.2471	62.14	0.98	0.841	0.12
4	0.2824	62.20	1.83	0.848	0.18
5	0.3177	62.46	7.28	0.856	0.23
6	0.33535	62.65	10.65	0.862	0.35
7	0.353	62.90	14.39	0.868	0.34
8	0.37065	63.18	15.75	0.875	0.40
9	0.3883	64.45	71.98	0.885	0.57
10	0.4236	65.88	40.63	0.895	0.28
Average			18.231		0.282

Table 6 shows that for acric ferralsol soils and the entire range of values of the soil water content under saturation conditions, the simulated peak flow and runoff coefficient decrease by $3.75 \text{ m}^3/\text{s}$ and 0.057, respectively, which are 5.69% and 6.39% decreases compared to their baseline values (ID = 1). The average sensitivity of peak flow is -17.469 , and the average sensitivity of the runoff coefficient is -0.245 . For the soil water content under field conditions, the average increase in the simulated peak flow and runoff coefficient are $3.80 \text{ m}^3/\text{s}$ and 0.0.06, respectively, which are 6.12% and 7.19% increases compared to their baseline values (ID = 1). The average sensitivity of peak flow is 18.231, and the average sensitivity of the runoff coefficient is 0.282. These sensitivity factors suggest that the sensitivities of the soil water contents under saturation and field conditions are similar for acric ferralsols.

Based on the above results and discussion, the runoff production process associated with acric ferralsol soils is a key hydrological process, and the soil water content under saturation conditions and soil water content under field conditions are sensitive parameters to this hydrological process. Therefore, the runoff production processes associated with both ferric luvisols and acric ferralsols are key hydrological processes, and their sensitive parameters include the soil water contents under saturation and field conditions. Thus, these parameters must be adjusted carefully.

5.3. Identify Key Runoff Routing Processes

Vegetation-based parameters include the evaporation coefficient and roughness. Since the evaporation coefficient is a less sensitive parameter compared to roughness, only sensitivity analysis to roughness was performed. The sensitivities of five LUC roughness, excluding that of water bodies, were analyzed individually, and 11 values were selected within acceptable ranges of values for each LUC. The simulated hydrographs based on these parameter values are shown in Figure 8a–e.

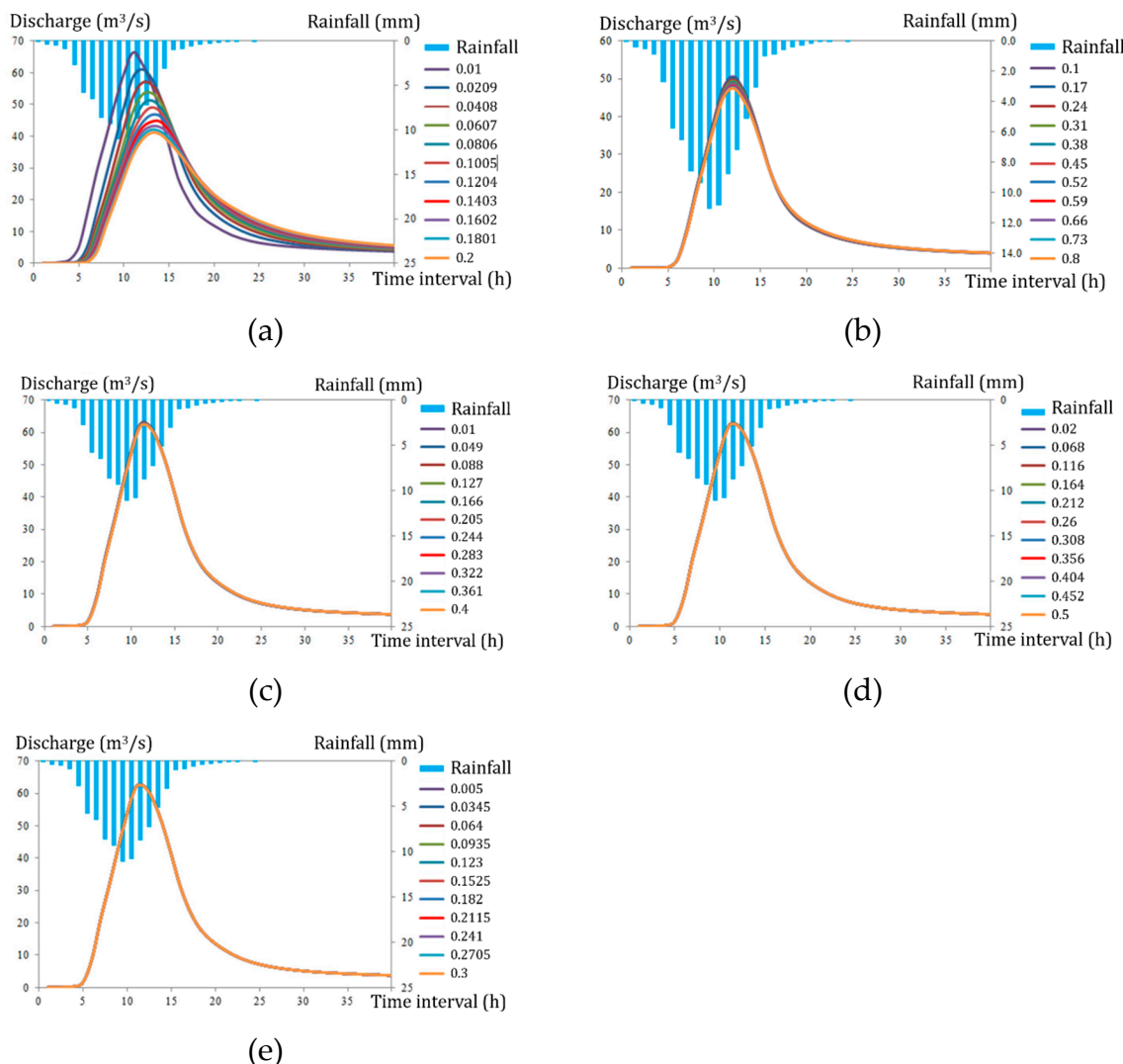


Figure 8. This simulated hydrographs for the roughness sensitivity analysis. (a) Urban land; (b) forestry land; (c) grassland; (d) farmland; (e) bare land.

Figure 8 shows that only the change in urban land roughness considerably influences the simulated hydrological process. Thus, only urban land roughness is a sensitive parameter in the Liuxihe model of Shahe Creek, and its value must be selected carefully. Based on the above results, the sensitivity factors of urban land roughness were calculated, and they are listed in Table 7. These sensitivity factors are only calculated for peak flow and the runoff coefficient.

Table 7 shows that for the entire range of values, the simulated peak flow decreases by $25.32 \text{ m}^3/\text{s}$, which is a decrease of 38.15% compared to its baseline value ($ID = 1$). Additionally, the runoff coefficient decreases by 0.097 over the entire range of values, which is a decrease of 11.11% compared to its baseline value ($ID = 1$). The average sensitivity factor of peak flow to urban land roughness is -141.40 , and the average sensitivity factor of the runoff coefficient to urban land roughness is -0.540 . Therefore, as roughness increases, the simulated peak flow and runoff coefficient decrease. The simulated peak flow changes significantly as the roughness changes, but the change in the runoff coefficient is not significant. Thus, roughness is more sensitive to peak flow.

Based on the above analysis, we conclude that only the runoff routing process associated with urban land is a key hydrological process, and only the roughness of urban land is a sensitive parameter that must be adjusted further.

Table 7. Sensitivity analysis results of urban land roughness.

ID	Roughness (%)	Peak Flow ($\text{m}^3 \cdot \text{s}^{-1}$)	Sensitivity Factor of Peak Flow ($\text{m}^3 \cdot \text{s}^{-1\%}^{-1}$)	Runoff Coefficient (no unit)	Sensitivity Factor of the Runoff Coefficient ($\% \cdot \%^{-1}$)
1	0.01	66.37		0.873	
2	0.029	61.10	-265.04	0.860	-0.624
3	0.048	56.81	-215.74	0.850	-0.536
4	0.067	53.70	-155.90	0.839	-0.534
5	0.086	51.31	-120.11	0.829	-0.490
6	0.105	49.07	-112.76	0.820	-0.495
7	0.124	46.66	-121.18	0.810	-0.487
8	0.143	44.64	-101.28	0.801	-0.454
9	0.162	43.09	-78.24	0.792	-0.439
10	0.181	42.01	-53.97	0.784	-0.416
11	0.2	41.05	-48.38	0.776	-0.387
Total			-141.40		-0.540

6. Parameter Adjust and Flood Simulation

6.1. Adjusting the Model Parameters of Key Hydrological Processes

Based on the above results and discussion, the key hydrological processes in highly urbanized watersheds are runoff production processes associated with both ferric luvisol and acric ferralsol soil types and the runoff routing process on urban land. The sensitive parameters include the soil water contents of the two soils under saturation and field conditions, as well as the roughness of urban land. The values of these sensitive parameters must be adjusted further using various methods.

In this study, the runoff coefficient is employed to adjust the sensitive parameters. Based on various references [81,84,85], the runoff coefficient in an urbanized watershed falls within the range of 0.5 to 0.7. This runoff coefficient range was proposed a few years ago and is out of date. Thus, a range of 0.6–0.85 is more reasonable considering recent urbanization. This range provides new information that can be used to adjust the sensitive parameters. If the simulated runoff coefficient falls within this range, then the model parameters are acceptable and can be used. Based on the results shown in Table 7, if the value of urban land roughness is within 0.048 to 0.2, then the simulated runoff coefficient is between 0.6 and 0.85. Thus, the value of urban land roughness should be limited to the range of 0.048 to 0.2. Similarly, the values of the soil water content under saturation conditions and soil water content under field conditions of ferric luvisols should be limited to 0.48 to 0.69 and 0.13 to 0.25, respectively. Additionally, the values of the soil water content under saturation conditions and soil water content under field conditions of acric ferralsols should be limited to 0.46 to 0.69 and 0.18 to 0.28, respectively. Based on this new information, which was compared to the initially proposed model parameters (Table 4), most of the soil-based parameters are outside the ranges of the above parameter values. Therefore, the final parameters were adjusted. The soil water content under saturation conditions and soil water content under field conditions of ferric luvisols were revised to 0.48 and 0.25, respectively. Additionally, the soil water content under saturation conditions and soil water content under field conditions of acric ferralsols were revised to 0.46 and 0.28, respectively. Finally, the urban land roughness was adjusted to 0.048.

6.2. Flood Simulations

Using the final Liuxihe model parameters for flood forecasting in the Shahe Creek watershed, three storms were simulated, and the simulated flood hydrographs are shown in Figure 9.

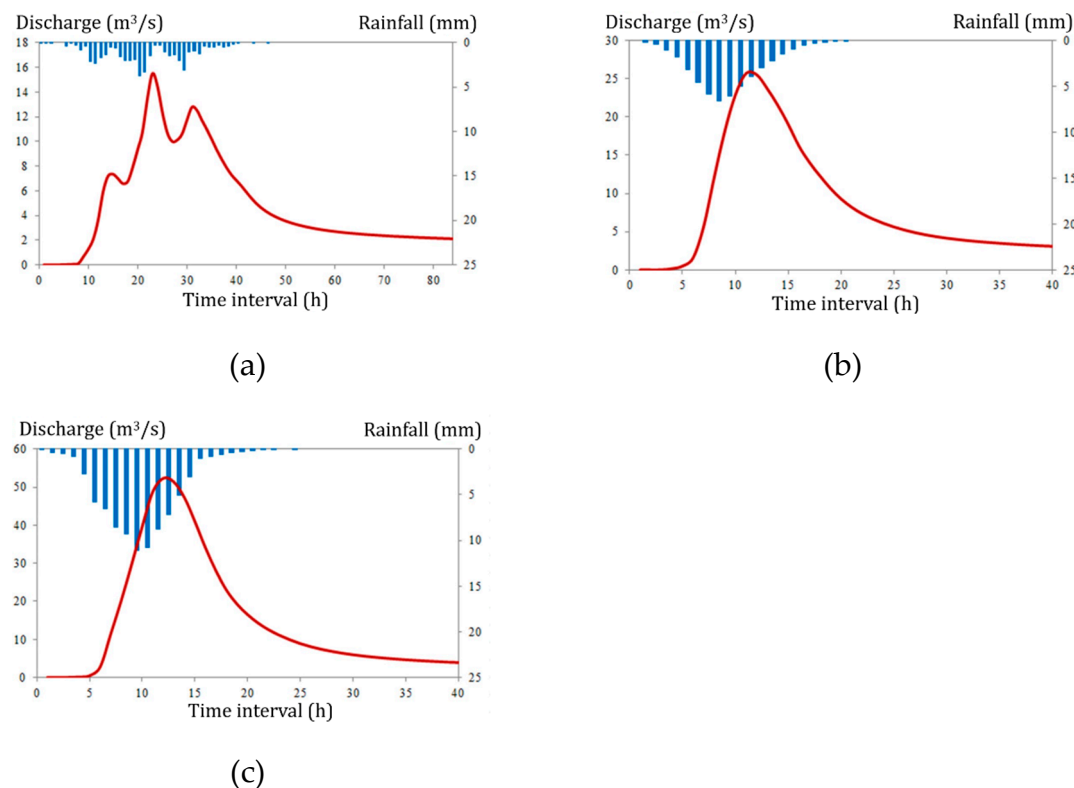


Figure 9. Simulated flood processes with proposed model parameters. (a) Flood 2015011118; (b) flood 2015051607; (c) flood 2016012813.

The runoff coefficients of the simulated flood processes for the three flood events are 0.686, 0.738 and 0.784. These values fall between 0.6 and 0.85; thus, the hydrographs accurately responded to precipitation, and the simulated hydrological processes can be regarded as reasonable. Additionally, the model parameters are acceptable and can be used for flood forecasting in the Shahe Creek watershed.

7. Conclusions

In this study, a procedure was proposed to identify key hydrological processes in highly urbanized watersheds for flood forecasting in the Pearl River Delta area, and a distributed hydrological model was used as the forecast tool. The procedure includes these steps: collecting the latest LUC information or estimating this information using satellite remote sensing images; analyzing LUC spatial patterns and identifying dominant LUC types and their spatial structures; choosing and establishing a distributed hydrological model as the forecasting tool and determining the initial model parameters; and identifying the key hydrological processes and sensitive model parameters based on a parameter sensitivity analysis. Finally, the sensitive model parameters are adjusted based on their initial values. A highly urbanized watershed flood hydrological process is studied with this procedure. Based on this study, the following conclusions have been proposed.

1. The Landsat 8 satellite remote sensing imagery taken on 3 January 2015 was used to estimate the LUC types in the Shahe Creek watershed. The urban land in Shahe Creek in 2015 comprises an areal percentage of 59.73% of the entire watershed; thus, it is the dominant LUC. Additionally, this value suggests that Shahe Creek is a highly urbanized watershed.

2. Runoff production processes associated with both ferric luvisol and acric ferralsol soil types are key hydrological processes, and the soil water content under saturation conditions and soil water content under field conditions are sensitive parameters. The runoff routing process on urban land is a key hydrological process, and the roughness of urban land is a sensitive parameter.

3. Local knowledge regarding runoff coefficients was used to adjust the sensitive model parameters related to key hydrological processes. In this study, the final values of the soil water content under saturation conditions and soil water content under field conditions of ferric luvisols were adjusted to 0.48 and 0.25, respectively. Additionally, the values of the soil water content under saturation conditions and soil water content under field conditions of acric ferralsols were adjusted to 0.46 and 0.28, respectively. Finally, urban land roughness was adjusted to 0.048.

Based on the above procedure, the key hydrological processes in a highly urbanized watershed and the associated sensitive parameters can be identified. Additionally, the sensitive parameters can be adjusted based on local knowledge, which can reduce the parameter uncertainty and make the model more appropriate for flood forecasting.

For an ungauged watershed, there is no hydrological data for calibrating or optimizing model parameters. Methodologies proposed for this kind of watershed flood forecasting employs some indirectly derived information to improve the model's performance. The method proposed in this paper uses the precipitation observation from rain gauges to make a parameter sensitivity analysis, then based on the local rainfall-runoff coefficient experiences, adjust the model parameters accordingly. It is expected that the model performance could be improved, but if the watershed has nothing in hydrological observations, this method cannot be used. Fortunately, in most of the urbanized watersheds in the world, this is true as installing rain gauges is affordable and not very expensive.

The above conclusion is mainly based on the application for flood forecasting, but the authors believe the method can also be used for other applications.

Author Contributions: Y.C. was responsible for proposing the original ideal and writing the paper; H.W. was responsible for the data compilation, processing, computation and drawing.

Funding: This study was supported by the National Key Research and Development Program of China (no. 2017YFC1502702), the National Science and Technology Pillar Program during the Twentieth Five-year Plan Period (no. 2015BAK11B02) and the Science and Technology Program of Guangdong Province (no. 2014A050503031).

Acknowledgments: We gratefully acknowledge the kind anonymous referees for their helpful comments.

Conflicts of Interest: The authors declare no conflicts of interest.

References

1. United Nations, Department of Economic and Social Affairs, Population Division. *World Population Prospects: The 2010 Revision*; United Nations: New York, NY, USA, 2010.
2. Rounsevell, M.D.; Reginster, I.; Araújo, M.B.; Carter, T.R.; Dendoncker, N.; Ewert, F.; House, J.I.; Kankaanpää, S.; Leemans, R.; Metzger, M.J.; et al. A coherent set of future land use change scenarios for Europe. *Agric. Ecosyst. Environ.* **2006**, *114*, 57–68. [[CrossRef](#)]
3. Fang, C.; Wang, D. Comprehensive development measuring and improving roadmap of China's urbanization quality. *Geogr. Res.* **2011**, *30*, 1931–1945.
4. Development Research Foundation of China. *Development Report of China*; People's Publishing: Beijing, China, 2011.
5. Li, W.; Chen, S.; Chen, G. Urbanization signatures in strong versus weak precipitation over the Pearl River Delta metropolitan regions of China. *Environ. Res. Lett.* **2011**, *6034020*. [[CrossRef](#)]
6. Chen, Y.; Zhou, H.; Zhang, H.; Du, G.; Zhou, J. Urban flood risk warning under rapid urbanization. *Environ. Res.* **2015**, *139*, 3–10. [[CrossRef](#)] [[PubMed](#)]
7. Zhang, M.; Liu, Y.; Wang, L. Inversion on Channel Roughness for Hydrodynamic Model by Using Quantum-Behaved Particle Swarm Optimization. *Yellow River* **2015**, *37*, 26–29.
8. Hollis, G.E. The Effect of urbanization on floods of different recurrence interval. *Water Resour. Res.* **1975**, *11*, 431–435. [[CrossRef](#)]
9. DeWalle, D.R.; Swistock, B.R.; Johnson, T.E.; McGuire, K.J. Potential effects of climate change and urbanization on mean annual streamflow in the United States. *Water Resour. Res.* **2000**, *36*, 2655–2664. [[CrossRef](#)]
10. Claessens, L.; Hopkinson, C.; Rastetter, E.; Vallino, J. Effect of historical changes in land use and climate on the water budget of an urbanizing watershed. *Water Resour. Res.* **2006**, *42*, W03426. [[CrossRef](#)]

11. Hurkmans, R.T.; Terink, W.; Uijlenhoet, R.; Moors, E.J.; Troch, P.A.; Verburg, P.H. Effects of land use changes on streamflow generation in the Rhine basin. *Water Resour. Res.* **2009**, *45*, W06405. [[CrossRef](#)]
12. Tu, J. Combined impact of climate and land use changes on streamflow and water quality in eastern Massachusetts, USA. *J. Hydrol.* **2009**, *379*, 268–283. [[CrossRef](#)]
13. Xie, Y.; Li, D.; Li, P.; Shen, S.; Yin, J.; Han, S.; Zeng, M.; Gu, X. Research and application of the mathematical model for urban rainstorm water logging. *Adv. Water Sci.* **2005**, *16*, 384–390.
14. Zhou, H.; Wang, C. Guangdong Dongguan city urban flooding causes analysis and prevention measures. *China Flood Drought Manag.* **2013**, *23*, 70–71.
15. Refsgaard, J.C.; Storm, B. Construction, calibration and validation of hydrological models. In *Distributed Hydrological Modelling*; Abbott, M.B., Refsgaard, J.C., Eds.; Kluwer Academic: Dordrecht, Holland, 1996; pp. 41–54.
16. Chen, Y.; Ren, Q.W.; Huang, F.H.; Xu, H.J.; Cluckie, I. Liuxihe Model and its modeling to river basin flood. *J. Hydrol. Eng.* **2011**, *16*, 33–50. [[CrossRef](#)]
17. Crawford, N.H.; Linsley, R.K. *Digital Simulation in Hydrology, Stanford Watershed Model IV*; Technical Report No. 39; Department of Civil Engineering, Stanford University: Stanford, CA, USA, 1966.
18. Zhao, R.J. *Flood Forecasting Method for Humid Regions of China*; East China College of Hydraulic Engineering: Nanjing, China, 1977.
19. Todini, E. The ARNO rainfall-runoff model. *J. Hydrol.* **1996**, *175*, 339–382. [[CrossRef](#)]
20. Freeze, R.A.; Harlan, R.L. Blueprint for a physically-based, digitally simulated, hydrologic response model. *J. Hydrol.* **1969**, *9*, 237–258. [[CrossRef](#)]
21. Abbott, M.B.; Bathurst, J.C.; Cunge, J.A.; O’Connell, P.E.; Rasmussen, J. An Introduction to the European Hydrologic System-System Hydrologue Europeen, ‘SHE’, a: History and Philosophy of a Physically-based, Distributed Modelling System. *J. Hydrol.* **1986**, *87*, 45–59. [[CrossRef](#)]
22. Abbott, M.B.; Bathurst, J.C.; Cunge, J.A.; O’Connell, P.E.; Rasmussen, J. An Introduction to the European Hydrologic System-System Hydrologue Europeen, ‘SHE’, b: Structure of a Physically based, Distributed Modeling System. *J. Hydrol.* **1986**, *87*, 61–77. [[CrossRef](#)]
23. Ambroise, B.; Beven, K.; Freer, J. Toward a generalization of the TOPMODEL concepts: Topographic indices of hydrologic similarity. *Water Resour. Res.* **1996**, *32*, 2135–2145. [[CrossRef](#)]
24. Kouwen, N. WATFLOOD: A Micro-Computer based Flood Forecasting System based on Real-Time Weather Radar. *Can. Water Resour. J.* **1988**, *13*, 62–77. [[CrossRef](#)]
25. Grayson, R.B.; Moore, I.D.; McMahon, T.A. Physically based hydrologic modeling: 1. A Terrain-based model for investigative purposes. *Water Resour. Res.* **1992**, *28*, 2639–2658. [[CrossRef](#)]
26. Liang, X.; Lettenmaier, D.P.; Wood, E.F.; Burges, S.J. A simple hydrologically based model of land surface water and energy fluxes for general circulation models. *J. Geophys. Res.* **1994**, *99*, 14415–14428. [[CrossRef](#)]
27. Wigmosta, M.S.; Vai, L.W.; Lettenmaier, D.P. A Distributed Hydrology-Vegetation Model for Complex Terrain. *Water Resour. Res.* **1994**, *30*, 1665–1669. [[CrossRef](#)]
28. Julien, P.Y.; Saghafian, B.; Ogden, F.L. Raster-Based Hydrologic Modeling of spatially-Varied Surface Runoff. *Water Resour. Bull.* **1995**, *31*, 523–536. [[CrossRef](#)]
29. Wang, Z.; Batelaan, O.; De Smedt, F. A distributed model for water and energy transfer between soil, plants and atmosphere (WetSpa). *J. Phys. Chem. Earth* **1997**, *21*, 189–193. [[CrossRef](#)]
30. Yang, D.; Herath, S.; Musiake, K. Development of a geomorphologic properties extracted from DEMs for hydrologic modeling. *Ann. J. Hydrol. Eng. JSCE* **1997**, *47*, 49–65.
31. Jia, Y.; Ni, G.; Kawahara, Y. Development of WEP model and its application to an urban watershed. *Hydrol. Process.* **2001**, *15*, 2175–2194. [[CrossRef](#)]
32. Vieux, B.E.; Vieux, J.E. VfloTM: A Real-time Distributed Hydrologic Model. In Proceedings of the 2nd Federal Interagency Hydrologic Modeling Conference, Las Vegas, NV, USA, 28 July–1 August 2002.
33. Kavvas, M.; Yoon, J.; Chen, Z.; Liang, L.; Dogrul, E.; Ohara, N.; Aksoy, H.; Anderson, M.; Reuter, J.; Hackley, S. Watershed Environmental Hydrology Model: Environmental Module and Its Application to a California Watershed. *J. Hydrol. Eng.* **2004**, *11*, 261–272. [[CrossRef](#)]
34. Kavvas, M.; Chen, Z.; Dogrul, C.; Yoon, J.; Ohara, N.; Liang, L.; Aksoy, H.; Anderson, M.; Yoshitani, J.; Fukami, K.; et al. Watershed Environmental Hydrology (WEHY) Model Based on Upscaled Conservation Equations: Hydrologic Module. *J. Hydrol. Eng.* **2002**, *9*, 450–464. [[CrossRef](#)]

35. Madsen, H. Parameter estimation in distributed hydrological catchment modelling using automatic calibration with multiple objectives. *Adv. Water Resour.* **2003**, *26*, 205–216. [[CrossRef](#)]
36. Smith, M.B.; Seo, D.-J.; Koren, V.I.; Reed, S.; Zhang, Z.; Duan, Q.Y.; Cong, S.; Moreda, F.; Anderson, R. The distributed model intercomparison project (DMIP): Motivation and experiment design. *J. Hydrol.* **2004**, *298*, 4–26. [[CrossRef](#)]
37. Pokhrel, P.; Yilmaz, K.K.; Gupta, H.V. Multiple-criteria calibration of a distributed watershed model using spatial regularization and response signatures. *J. Hydrol.* **2012**, *418–419*, 49–60. [[CrossRef](#)]
38. Chen, Y.; Li, J.; Xu, H. Improving flood forecasting capability of physically based distributed hydrological model by parameter optimization. *Hydrol. Earth Syst. Sci.* **2016**, *20*, 375–392. [[CrossRef](#)]
39. Apel, H.; Thielen, A.H.; Merz, B.; Blöschl, G. Flood risk assessment and associated uncertainty. *Nat. Hazards Earth Syst. Sci.* **2004**, *4*, 295–308. [[CrossRef](#)]
40. Moradkhani, H.; Hsu, K.-L.; Gupta, H.; Sorooshian, S. Uncertainty assessment of hydrologic model states and parameters: Sequential data assimilation using the particle filter. *Water Resour. Res.* **2005**, *41*. [[CrossRef](#)]
41. Liu, Y.; Gupta, H.V. Uncertainty in hydrologic modeling: Toward an integrated data assimilation framework. *Water Resour. Res.* **2007**, *43*. [[CrossRef](#)]
42. Apel, H.; Merz, B.; Thielen, A.H. Quantification of uncertainties in flood risk assessments. *Int. J. River Basin Manag.* **2008**, *6*, 149–162. [[CrossRef](#)]
43. Beven, K. Facets of uncertainty: Epistemic uncertainty, non-stationarity, likelihood, hypothesis testing, and communication. *Hydrol. Sci. J.* **2016**, *61*, 1652–1665. [[CrossRef](#)]
44. Vieux, B.E.; Moreda, F.G. Ordered physics-based parameter adjustment of a distributed model. In *Advances in Calibration of Watershed Models*; Water Science and Application Series; Duan, Q., Sorooshian, S., Gupta, H.V., Rousseau, A.N., Turcotte, R., Eds.; American Geophysical Union: Washington, DC, USA, 2003; Volume 6, pp. 267–281.
45. Vieux, B.E.; Cui, Z.; Gaur, A. Evaluation of a physics-based distributed hydrologic model for flood forecasting. *J. Hydrol.* **2004**, *298*, 155–177. [[CrossRef](#)]
46. Shafii, M.; Smedt, F.D. Multi-objective calibration of a distributed hydrological model (WetSpa) using a genetic algorithm. *Hydrol. Earth Syst. Sci.* **2009**, *13*, 2137–2149. [[CrossRef](#)]
47. Xu, H.; Chen, Y.; Zeng, B.; He, J.; Liao, Z. Application of SCE-UA Algorithm to Parameter Optimization of Liuxihe Model. *Trop. Geogr.* **2012**, *32*, 32–37.
48. Dou, P.; Chen, Y. Dynamic monitoring of land-use/land-cover change and urban expansion in Shenzhen using Landsat imagery from 1988 to 2015. *Int. J. Remote Sens.* **2017**, *38*, 5388–5407. [[CrossRef](#)]
49. Chen, Y.; Dou, P.; Yang, X. Improving Land Use/Cover Classification with a Multiple Classifier System Using AdaBoost Integration Technique. *Remote Sens.* **2017**, *9*, 1055. [[CrossRef](#)]
50. Chen, Y.; An, X.; Dou, P.; Zhang, T. Estimating Land Use/Cover of Foshan City in Southern China with Landsat Remote Sensing Imagery for Flood Modeling. In Proceedings of the International Multidisciplinary Scientific GeoConference Surveying Geology and Mining Ecology Management, SGEM, Albena, Bulgaria, 27 June–6 July 2017; Volume 17, pp. 79–86.
51. Chen, Y. *Liuxihe Model*; Science Press: Beijing, China, 2009; 198p.
52. Langley, P.; Sage, S. Induction of selective Bayesian classifiers. In Proceedings of the Tenth Conference on Uncertainty in Artificial Intelligence, Seattle, WA, USA, 29–31 June 1994; Morgan Kaufmann: San Francisco, CA, USA, 1994.
53. Pal, M.; Mather, P.M. An assessment of the effectiveness of decision tree methods for land cover classification. *Remote Sens. Environ.* **2003**, *86*, 554–565. [[CrossRef](#)]
54. Kavzoglu, T.; Mather, P.M. The use of back propagating artificial neural networks in land cover classification. *Int. J. Remote Sens.* **2003**, *24*, 4907–4938. [[CrossRef](#)]
55. Zhu, G.B.; Blumberg, D.G. Classification using ASTER data and SVM algorithms: The case study of Beer Sheva, Israel. *Remote Sens. Environ.* **2002**, *80*, 233–240. [[CrossRef](#)]
56. Mazzoni, D.; Garay, M.J.; Davies, R.; Nelson, D. An operational MISR pixel classifier using support vector machines. *Remote Sens. Environ.* **2007**, *107*, 149–158. [[CrossRef](#)]
57. Gomez-Chova, L.; Camps-Valls, G.; Munoz-Mari, J.; Calpe, J. Semisupervised image classification with Laplacian support vector machines. *IEEE Geosci. Remote Sens. Lett.* **2008**, *5*, 336–340. [[CrossRef](#)]
58. Ding, Z.J.; Yu, J.; Zhang, Y. A New Improved K-Means Algorithm with Penalized Term. In Proceedings of the IEEE International Conference Granular Computing, Fremont, CA, USA, 2–4 November 2007; pp. 313–317.

59. Thitimajshima, P. A New Modified Fuzzy C-Means Algorithm for MULTISPECTRAL satellite Images Segmentation. In Proceeding of the IGARSS, Honolulu, HI, USA, 24–28 July 2000; Volume 4, pp. 1684–1686.
60. Yang, C.; Bruzzone, L.; Sun, F.Y.; Lu, L.J.; Guan, R.C.; Liang, Y.C. A Fuzzy-Statistics-Based Affinity Propagation Technique for Clustering in Multispectral Images. *IEEE Trans. Geosci. Remote Sens.* **2010**, *48*, 2647–2659. [[CrossRef](#)]
61. Shahshahani, B.; Landgrebe, D. The effect of unlabeled samples in reducing the small sample size problem and mitigating the huge sphenomenon. *IEEE Trans. Geosci. Remote Sens.* **1994**, *32*, 1087–1095. [[CrossRef](#)]
62. Nigam, K.; McCallum, A.; Thrun, S. Text classification from labeled and unlabeled documents using EM. *Mach. Learn.* **1999**, *39*, 103–134. [[CrossRef](#)]
63. Blum, A.; Mitchell, T. Combining Labeled and Unlabeled Data with Co-Training. In Proceedings of the Computer Learning Theory, Madison, WI, USA, 24–26 July 1998; pp. 92–100.
64. Tuia, D.; Camps-valls, G. Semi-supervised remote sensing image classification with cluster kernels. *IEEE Geosci. Remote Sens. Lett.* **2009**, *6*, 224–228. [[CrossRef](#)]
65. Vapnik, V.N. Statistical Learning Theory. *Encycl. Sci. Learn.* **2010**, *41*, 3185.
66. Nemmour, H.; Chibani, Y. Multiple support vector machines for land cover change detection: An application for mapping urban extensions. *Isprs J. Photogramm. Remote Sens.* **2006**, *61*, 125–133. [[CrossRef](#)]
67. Demarchi, L.; Canters, F.; Cariou, C.; Licciardi, G.; Chan, J.C. Assessing the performance of two unsupervised dimensionality reduction techniques on hyperspectral APEX data for high resolution urban land-cover mapping. *Isprs J. Photogramm. Remote Sens.* **2014**, *87*, 166–179. [[CrossRef](#)]
68. Saltelli, A.; Ratto, M.; Tarantola, S.; Campolongo, F. Sensitivity analysis practices: Strategies for model-based inference. *Reliab. Eng. Syst. Saf.* **2006**, *91*, 1109–1125. [[CrossRef](#)]
69. Irons, J.R.; Dwyer, J.L.; Barsi, J.A. The next Landsat satellite: The Landsat data continuity mission. *J. Remote Sens. Environ.* **2012**, *122*, 11–21. [[CrossRef](#)]
70. Tang, H.Q.; Xu, F. Analysis of new characteristics of the first Landsat 8 image and their Ecoenvironmental significance. *Acta Ecol. Sin.* **2013**, *33*, 3249–3257.
71. O’Callaghan, J.; Mark, D.M. The extraction of drainage networks from digital elevation data. *Comput. Vis. Graph. Image Process* **1984**, *28*, 323–344. [[CrossRef](#)]
72. Jensen, S.K.; Domingue, J.O. Extracting Topographic Structure from Digital Elevation Data for Geographic Information System Analysis. *Photogramm. Eng. Remote Sens.* **1988**, *54*, 1593–1600.
73. Strahler, A.N. Quantitative Analysis of watershed Geomorphology. *Trans. Am. Geophys. Union* **1957**, *38*, 913–920. [[CrossRef](#)]
74. Chen, H.; Mao, S. Calculation and Verification of an Universal Water Surface Evaporation Coefficient Formula. *Adv. Water Sci.* **1995**, *6*, 116–120.
75. Zhang, S.; Xu, D.; Li, Y.; Cai, L. An optimized inverse model used to estimate Kostiakov infiltration parameters and Manning’s roughness coefficient based on SGA and SRFR model: I Establishment. *J. Hydraul. Eng.* **2006**, *11*, 1297–1302.
76. Zhang, S.; Xu, D.; Li, Y.; Cai, L. Optimized inverse model used to estimate Kostiakov infiltration parameters and Manning’s roughness coefficient based on SGA and SRFR model: II Application. *J. Hydraul. Eng.* **2007**, *4*, 402–408.
77. Guo, H.; Hua, Y.; Bai, X. Hydrological Effects of Litter on Different Forest Stands and Study about Surface Roughness Coefficient. *J. Soil Water Conserv.* **2010**, *24*, 179–183.
78. Li, Y.; Zhang, J.; Ru, H.; Li, M.; Wang, D.; Ding, Y. Effect of Different Land Use Types on Soil Anti-scorability and Roughness in Loess Area of Western Shanxi Province. *J. Soil Water Conserv.* **2013**, *27*, 1–6.
79. Zaradny, H. *Groundwater Flow in Saturated and Unsaturated Soil*; A A Balkema: Now York, NY, USA, 1993.
80. Anderson, A.N.; McBratney, A.B.; FitzPatric, K.E. A soil mass, surface and spectral fractal dimensions estimated from thin section photographs. *Soil Sci. Soc. Am. J.* **1996**, *60*, 962–969. [[CrossRef](#)]
81. Shen, S.; Guze, S. Conversion Coefficient between Small Evaporation Pan and Theoretically Calculated Water Surface Evaporation in China. *J. Nanjing Inst. Meteorol.* **2007**, *30*, 561–565.
82. Arya, L.M.; Paris, J.F. A physioempirical model to predict the soil moisture characteristic from particle-size distribution and bulk density data. *Soil Sci. Soc. Am. J.* **1981**, *45*, 1023–1030. [[CrossRef](#)]
83. Liu, H. *Fluid Mechanics*; China Architecture and Building Press: Beijing, China, 2001.

84. Liu, X. Parameter calibration method for urban rainfall-runoff model based on runoff coefficient. *Water Wastewater Eng.* **2009**, *11*, 213–217.
85. He, B.; Chen, C.; Zhou, N. Urbanized Area Runoff Coefficient and its Application. *Shanghai Environ. Sci.* **2003**, *7*, 472–516.



© 2019 by the authors. Licensee MDPI, Basel, Switzerland. This article is an open access article distributed under the terms and conditions of the Creative Commons Attribution (CC BY) license (<http://creativecommons.org/licenses/by/4.0/>).